Forschung im Ingenieurwesen (2025)89:157
https://doi.org/10.1007/s10010-025-00924-w

ORIGINALARBEITEN/ORIGINALS

Design of a sensor integrating bolt for multiaxial force measurement and development of a design methodology

David Riehl[1] · Julian Peters[2] · Felix Herbst[3] · Dirk Leiacker[1] · Mario Kupnik[3] · Sven Matthiesen[2] · Klaus Hofmann[1]

Received: 2 April 2025 / Accepted: 29 September 2025

Abstract

Structurally integrated force measurements enable real-time monitoring of the overall system status. Existing sensor integration strategies in bolts often compromise mechanical integrity and deviate from standardized external dimensions, limiting their applicability. In this paper, a sensor is presented that is integrated into a M20 bolt to measure axial force and bending torques. The sensor is integrated directly into the bolt itself without altering its external dimensions. This integration method offers a more flexible solution compared to currently available solutions. Furthermore a method is presented that is extracted out of the development process. It includes the optimization of the design space for sensor and electronics as well as a general procedure based on the VDI 2206 and the methodology of testing. The sensor-integrating bolt retains 76.5% of the static load capacity of a standard bolt, which can be compensated by selecting a higher strength class. The sensor body consists of three vertical bending beams with applied strain gauges. The experimental findings have revealed a low linearity error of ±0.82% for axial load and ±0.11% for bending load. Linearity errors were measured at ±1.53% and ±0.52%, respectively. A flexible modular electronic platform has been developed, suited for complete integration into the bolt's head. It allows experimentation with the sensors read-out electronics, and various modules for communication. The energy supply is evaluated using different energy harvesting and energy transmission concepts. The novel sensor integrating bolt can be used to measure all relevant loads on bolts and to indicate early failure like decrease of clamping force or opening joints. The method can be used to support future sensor integration projects.

1 Introduction

Digitization progresses in industry and beyond are focusing on using data to improve the performance of machines and systems. The foundation for this lies in the comprehensive collection and analysis of data that reflect the condition of machines [1]. Only then can the benefits of approaches such as condition monitoring (CM) or structural health monitoring (SHM) be fully exploited. In particular, in-situ data captured at process-relevant locations enables reliable assessments of both machine condition and operational processes, as demonstrated in research on gearboxes, hydraulic systems, and additively manufactured components [2–5]. There is a lack of compact, autonomous and easy-to-use sensors that can be installed on site with reasonable effort [6, 7].

✉ Julian Peters
julian.peters@kit.edu

David Riehl
david.riehl@tu-darmstadt.de

Felix Herbst
felix.herbst@tu-darmstadt.de

Dirk Leiacker
dirk.leiacker@tu-darmstadt.de

Mario Kupnik
mario.kupnik@tu-darmstadt.de

Sven Matthiesen
sven.matthiesen@kit.edu

Klaus Hofmann
klaus.hofmann@tu-darmstadt.de

[1] Integrated Electronic Systems Lab, Technische Universität Darmstadt, Merckstr. 25, 64283 Darmstadt, Hessen, Germany

[2] Institute of Product Engineering, Karlsruher Institute of Technology, Gotthard-Franz-Str. 9, 76131 Karlsruhe, Baden-Württemberg, Germany

[3] Measurement and Sensor Technology Group, Technische Universität Darmstadt, Merckstr. 25, 64283 Darmstadt, Hessen, Germany

Published online: 23 October 2025

Table 1 Comparison of the state of the art of sensor principles for bolt monitoring

Sensor element, principle, location	Target measurement and physical quantity	Data acquisition/ transmission & energy transfer	Influence on mechanical functionality	Installation space neutrality/preservation of mechanical interfaces	Sources
Strain gauge on bolt head	Uniaxial preload force (static and dynamic) by strain on head	Wireless RFID	None	No	[16]
Thin-film sensor technology in washer	Preload force by change in pressure on the sensor layer, temperature	Wireless LPWAN; solar cells	None	No	[17, 18]
Strain gauges on deformation body in bolt shaft	Axial force by strain	Wired plug connection on bolt's head	No statement	No	[10]
Piezoceramic tube under prestress in bolt shaft	Uniaxial force by piezoelectric load charge	Wired plug connection on bolt's head	No statement	No	[19, 20]
Strain gauges in central cavity of cylinders	Multiaxial force by strain, temperature, acceleration	Wireless BLE, integrated energy storage	Yes	Yes	[21]
Strain gauge in thread root	Axial force by strain	Wired plug connection on bolt	None	No	[22]
Analog measuring pin on bolt head	Axial force by difference between measuring pin and bolt head (optical)	External, wireless measuring electronics	None	No	[23]
Ultrasound on bolt head	Axial force by ultrasonic pulse transition time	External, wired measuring electronics	None	No	[24]
Capacitive sensor under thread	Pull out length by capacitance change	External, wired measuring electronics	None	No	[25]

This gap in comprehensive measurement data acquisition can be addressed by integrating sensor capabilities into machine elements, thereby creating sensor-integrating machine elements (SiME) [8]. Standardized machine elements are installed in almost every technical system, so they have great potential in the form of a SiME for the in-situ acquisition of meaningful measurement data. Therefore, SiME are researched within the priority program SPP2305, funded by the German Research Foundation [9].

1.1 Sensor integration into bolts

Sensor integration in metric bolts offers great potential, as bolts are among the most commonly used machine elements and are typically situated in the force flow [10]. This enables the prediction of system states from the bolt's measurement data. There are several applicable standards for metric bolts, such as DIN 13-1 [11] for specifying the thread, DIN EN ISO 4014 [12] for specifying hexagon head shapes and shanks and VDI 2230 sheet 1 [13] for designing bolt connections. Sensor integrating bolts (SiS) must comply with these standards to ensure broad usability and allow retrofitting. Bolts are generally subjected to multiaxial loads [10]. During conventional tightening, the torsional torque is superimposed with tensile forces. Additional tensile forces and bending torques can occur during operation [14]. This makes a multiaxial force measurement necessary in order to fully record the condition of the bolt. According to Templeman et al. [15] there is a multiaxial force measurement if forces and torques occurring in more than one spatial direction are measured. In summary, the following requirements for sensor-integrated bolts must be met in order to measure relevant load cases and comply with the standards and guidelines:

- Maintain the mechanical function of the bolt, demonstrate the reliability of the SiS,
- Maintain standardized mechanical interfaces (head, thread, outer diameter) (installation space neutrality),
- Provide wireless power and data transmission to ensure easy integration,
- Provide measurement data for all relevant load cases (multiaxial force measurement for bolts).

An overview of the current state of research on SiME was compiled in Kirchner et al. in collaboration with the authors [6]. The part relevant to SiS is presented below (Table 1). These can be categorized according to the following points:

1. sensor principle and location;
2. measured physical quantities;
3. data acquisition and transmission;

4. influence on mechanical functionality and mechanical interfaces.

To summarize the Table 1, it can be stated that although bolts that integrate sensors already exist, they have individual disadvantages, which are summarized below:

- Sensor-bolt is limited to a single component measurement (axial force), no sufficient measurement of bending load cases [10, 16, 19, 20, 22, 24, 25];
- Impairment of the mechanical function, limits applicability of the machine element [21];
- Modification of the mechanical interfaces (cable-bound), makes installation more difficult, especially retrofitting [10, 16–20, 22, 24, 25];
- Energy management—operation of the sensor system over its service life is limited to special installation situations, generally not possible over the service life of the machine element; also existing solutions limit applicability to specific environment conditions like sunlight for solar cells, for example [17, 18];

In general, a systematic approach and methodical support for integrating sensor technology, particularly when addressing conflicting objectives during design space identification, are currently lacking [6, 26].

1.2 Research status of energy-autonomous sensor systems

It is crucial to minimize energy consumption for measurement, processing, and transmission, in order to ensure that the sensor system runs for as long as possible. This is mainly achieved by minimizing active operating times and turning off subsystems that are not required. However, in order to switch on individual subsystems at regular intervals, a permanently active timer is required, the energy consumption of which cannot be neglected throughout the life cycle of the machine element [27]. By using zero power wake-up systems, which require very little to no energy in the idle state, this can be dispensed with and the electronics can be activated by a defined event such as acceleration, vibration or reception of an RF signal [28].

Various technologies are widely used to generate energy from environmental influences and cover the energy demand. These include solar cells [29], Peltier elements for temperature differences, spring-mass oscillators or piezoelectric bending beams for mechanical energy [30] and high-frequency rectifiers for electromagnetic energy [31]. Targeted energy transfer is also possible. Robust and efficient inductively coupled systems are suitable for short distances (< 2 cm) [32, 33]. RFID systems based on electromagnetic waves are used for distances of up to 10 m and very low power requirements [34]. Another option for machine elements is acoustic energy transfer through solid bodies [35]. This enables full encapsulation of the sensor technology within the metallic SiME. However, the applicability in the sensor bolt needs to be researched.

Sensor data transmission and sensor system configuration are achieved through the use of energy transmission channels (e.g., NFC, RFID, Qi) or low-energy radio protocols (e.g., BLE, LoRa, ZigBee). The former uses techniques such as load modulation or modulation of a second carrier frequency for communication [32–36]. Classic wireless protocols offer higher data rates and extend transmission distances. However, these come with the downside of increased energy consumption and the necessity of integrating an antenna. Reliable transmission cannot always be guaranteed, especially in industrial environments [34, 37].

1.3 Objective of this paper

The objective of the first funding period within the SPP2305 (FP 1) was to design and solve the interdisciplinary research issues of a sensor-integrating bolt (SiS) with multiaxial force measurement and self-sufficient energy supply throughout the service life. The integration of the sensor should not affect the mechanical interfaces of the bolt (neutrality of the installation space), which means that the sensor and the electronics to acquire and communicate the data must be integrated within the bolt (Fig. 1). Furthermore, the influence on the mechanical function of the machine element, in the case of the bolt connection the application of clamping force, should be minimized. The procedure for achieving this goal is also used to extend existing design methods for mechatronic systems, specifically for the development of sensor-integrating machine elements.

To this end, the work described here as part of FP 1 of the SPP2305 investigated a SiS with the principle of multiaxial force measurement based on strain gauges (SG). For this purpose, the overall objective was divided into four subobjectives, listed below.

1. Identification of design space
2. Sensor concept and integration of sensor into bolt
3. Electronics for acquiring and transferring measurement data
4. Develop a methodical approach to support sensor integration into machine elements

The development process is based on the VDI 2206 [38], combining three experts from bolt mechanics, sensors and electronics. Starting with the analysis of the conventional machine element, the sensor integration was carried out step by step with increasing degree of integration. The process involves iterative development, the usage of testing objects with increasing complexity and structured testing.

The objectives and their solution are described in detail in the next chapters, followed by a conclusion.

2 Design space identification

In order to ensure widespread usage of the SiS, the sensor integration should not affect the standardized mechanical interfaces of the bolt and should have as little influence as possible on the mechanical function of the bolt, which is to apply clamping force. Therefore the sensor needs to be integrated into cavities inside the bolt. As cavity dimensions parameters d_1,d_2,h_1,h_2 are defined (Fig. 2).

Meanwhile, the novel sensor function should be able to measure multiaxial force with little errors and provide measurements throughout the service life of a conventional bolt. This leads to a conflict of objectives which is summarized in the following:

1. the fulfillment of the mechanical function of the bolt, applying clamping force, which is weakened by the cavities—the smaller the cavities, the lesser the influence on the mechanical function,
2. the fulfillment of the sensor function—every load condition on the bolt must be converted into a strain on the strain gauge-based sensor—the larger the cavities (especially the diameter), the higher the strain, thus a better the measurement signal.

The conflict of objectives is resolved by analyzing and modeling the effects of the design space parameters on the mechanical and sensory function, taking into account the effective structure. A mathematical model is created that takes into account the deformation state of the bolt. It integrates the mechanical function fulfillment, parameterized by the v. Mises stress, and the sensory function fulfillment, parameterized by the strain at the sensor position. Stress is a commonly used for evaluating the mechanical behavior, thus enables comparability [14, 39, 40]. Furthermore, the remaining force bearing capability of the bolt can be calculated with the known geometry and material parameters. Stress and strain are taken from the results of a finite element (FE) analyses. For the model, mathematical functions are derived from the FE data using curve fitting. The functions describe the increase of v. Mises stress and strain with respect to the cavity dimensions. An optimizable mathematical function is created, minimizing the v. Mises stress increase and the inverse of the strain increase. This leads to a design space solution. The procedure was recently published in [41] and is depicted in Fig. 2. The FE model is shown in Fig. 3, as published in [41].

The optimal design space parameters for the integration of electronics and sensors, depending on the fulfillment of the function, are shown in Fig. 4 published as part of the project [41, 42].

The mechanical and sensory parts of the fulfillment of the function are combined within one function (symbol O, Eq. 1) with respect to the parameters of the design space. Weighting factors w_{mech}, w_{sens} are introduced to allow prioritization (Eq. 2). An exponential approach for the optimization function is used. To achieve better alignment and obtain more feasible weights, the subcomponents $\sigma_{v,max}, \varepsilon_{shaft}$ are normed, as shown by Sahib et al. [43]. The strain part ε_{shaft} is inverted to obtain an opposing behavior to monotonously rising $\sigma_{v,max}$. The boundary condition of mountability $d_2 > d_1$ is shown as a black line in Fig. 4. This was published in [41].

$$\mathrm{O}(d_1, d_2) := exp\left(w_{mech}\frac{\sigma_{v,max}(d_1,d_2)}{\sigma_{v,max}(0,0)}\right) \cdot exp\left(w_{sens}\frac{\varepsilon_{shaft}(0,0)}{\varepsilon_{shaft}(d_1,d_2)}\right) \tag{1}$$

$$w_{mech} = [0..1] \qquad w_{sens} = 1 - w_{mech} \tag{2}$$

The results can be used to determine absolute strain values, from which the deformation state at the sensor position and, together with a minimum force or torque to be resolved, requirements for the rest of the measuring chain can be derived. This includes the measuring bridge and the effective number of bits (ENOB) of the analog digital converter (ADC) [41].

The strain outputs of the FE model were verified in empirical tests. Strain gauges were applied to defined positions on the bolt and then the bolt was subjected to load in a universal testing machine. The results of the strains were compared to the corresponding nodes of the FE model sim-

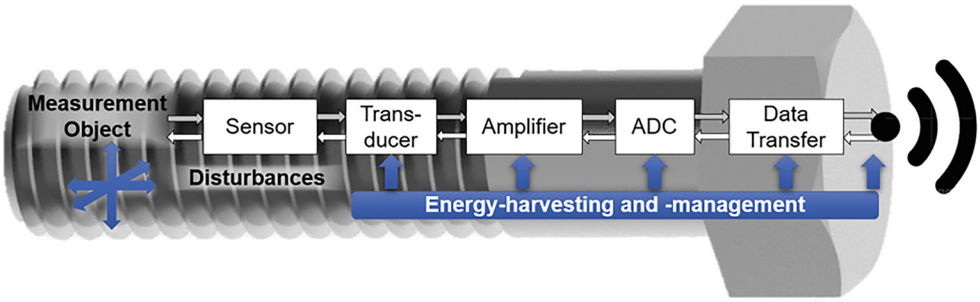

Fig. 1 Graphical representation of the idea followed in this project to integrate all components necessary for multiaxial force measurement into the bolt

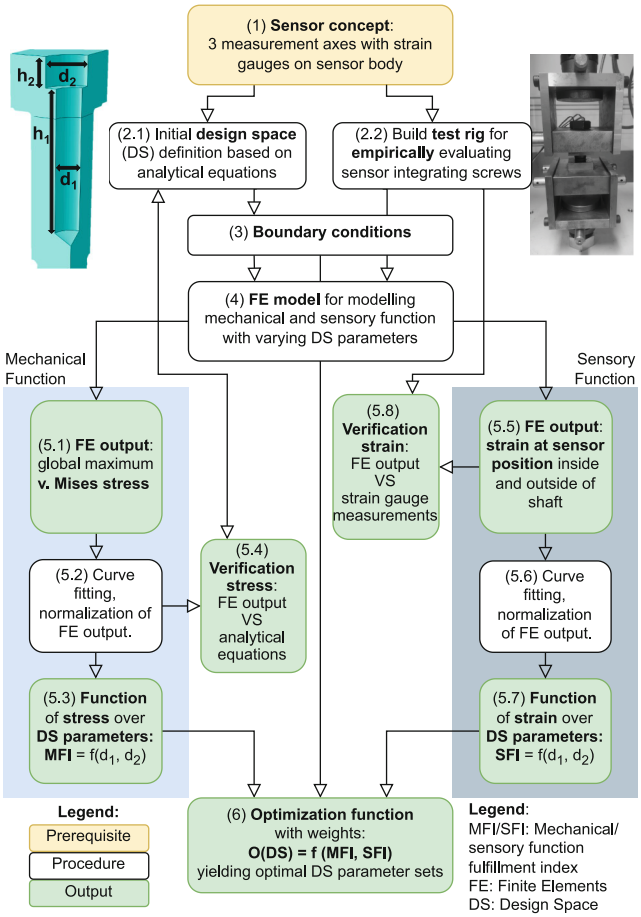

Fig. 2 Procedure for design space identification by composing an optimization function including models of mechanical and sensory function fulfillment, based on [41]. Steps 1–4 concern the definition of a sensor concept (e.g. strain gauges) and initial design space dimensions. Boundary conditions are set and subsequently the FE model is built, which is the base for the mathematical models in the following. From step 5 the procedure splits in the mechanical (v. Mises stress) and sensory part (strain): The change of these quantities due to cavity dimensions is analyzed and fitted into mathematical functions using curve fitting for each part. Certain points are verified by analytical calculations and physical testing using strain gauges. Finally, in step 6 an optimizable function is constructed out of the functions to retrieve solutions for the cavity dimensions (design space parameters)

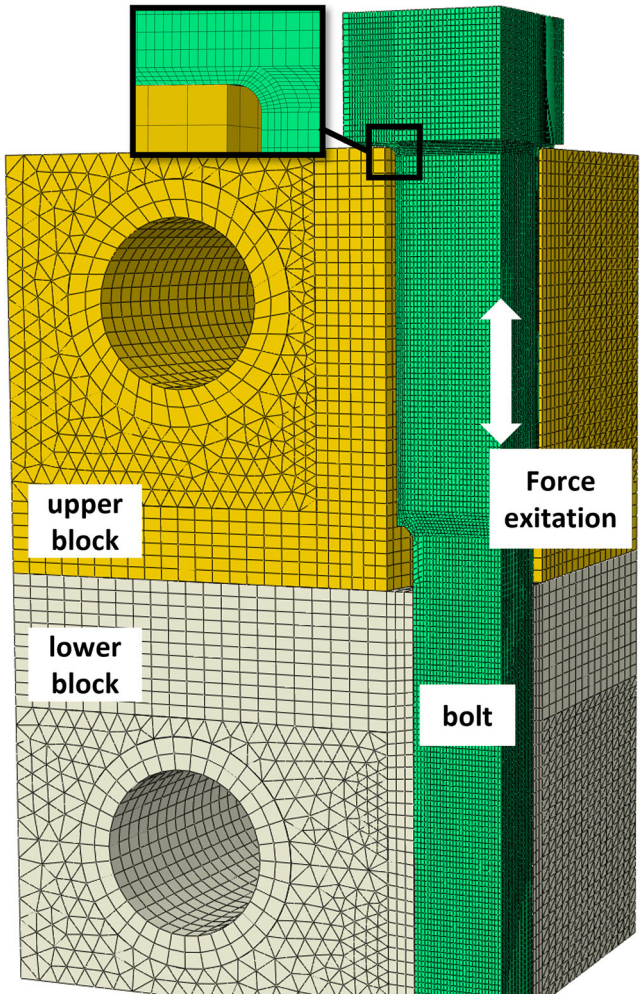

Fig. 3 FE model for evaluating the v. Mises stress and strain under the influence of sensor integration, taken from [41]

ulation. The results show a similar behavior with relative errors less than 20% of the true value for forces greater than a load of 30 kN.

The presented design space optimization procedure is transferable to other machine elements, which was shown on the example of bolts with smaller size M12 and an elastomer coupling, both fellow subprojects within the SPP2305, published in [44]. The procedure yielded viable results: For the bolt the conflict of objectives between mechanical and sensory function was similar and could be solved producing a diameter and height for a borehole to integrate sensors and electronics. For the coupling no conflict of objectives existed with the parameters investigated, so an optimization was not necessary. However, the influence of the design space parameters on the mechanical and sensory function could be quantified and new boundary conditions were discovered, aiding to take better design space decisions [44].

3 Sensor design and evaluation

In this section, we present the sensor design. For a better understanding of the derived design methodology, the following chapter includes brief outlines of the preliminary tests, development steps, and prototypes that led to the final result, published under [45, 46]. Details can be found in those publications, here we present an overview. Subsequently, we describe the measurement setup used to characterize the standalone sensor and discuss the corresponding results. Finally, we introduce the integration in the sensor-integrating bolt, detail the measurement procedure within

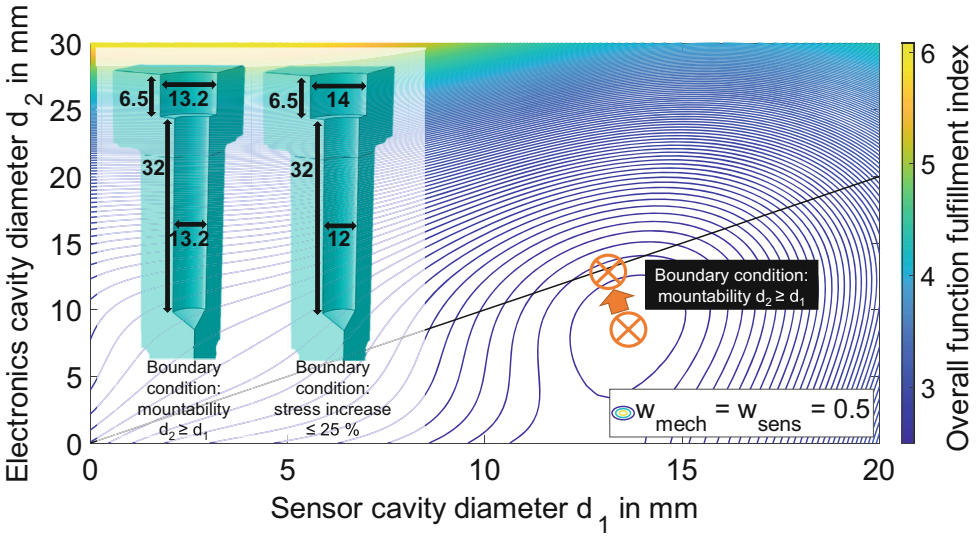

Fig. 4 Identification of optimal design space parameters for sensor and electronics with mountability boundary conditions (black line) and $w_{mech} = w_{sens} = 0.5$. Design space parameters d_1, d_2 are shown here because of their higher influence compared to the heights. Two design space parameter possibilities are shown, one without any other boundary conditions apart from mountability, the other one with stress increase limited to 25%. The figure is based on [41]

the bolt, and conclude the section with a discussion of the results obtained integrated in the bolt.

3.1 Sensor design

A custom sensor was designed, limited by the determined design space (Sect. 2) and required to measure both axial forces and bending torques in the full working range of the M20 bolt. Three sensor prototypes were built in three iterations, starting with the simplest possible preliminary tests and ending with the sensor that was ultimately installed in the bolt and meets all requirements. In the following section, we will only briefly present the results of the preliminary tests and focus primarily on the results of the final prototype.

The first test was used to identify the measurement principle. Three cylindrical strain gauges (TB21, HBK, Darmstadt, Germany) are applied to three bores in the shaft of the bolt, symmetrically spaced at 120 °C (Fig. 5).

The HBK TB21 strain gauge elements are based on conventional strain gauges that are rolled into a cylindrical shape, making them specifically designed for easy insertion into a bore. The measurement results obtained confirm the basic applicability of the principle. However, the temperature dependency of these rolled strain gauges showed a non-linear behavior and a remaining drift. This is most likely caused by the glue layer, whose thickness can hardly be controlled because there is no possibility to apply pressure while curing.

The second prototype is intended to improve the installation of the strain gauges by enabling better alignment and the application of pressure while curing. Therefore, the sensor is manufactured separately from the bolt and assembled afterwards. The sensor body is a cylindrical body with three flattened surfaces to which strain gauges (N5K-06-S5045H, Micro-Measurements supplied via ME-Systeme, Germany) with individual grids were attached in a half bridge configuration (Fig. 6). This sensor body is then pressed into the bolt (Fig. 6). Results demonstrate that the sensor is able to measure multiaxial forces with large hysteresis error. The hysteresis error was found to be caused by a failing interference fit. The required strain transmission from bolt to sensor was compromised. Also, the sensitivity of bending torques is too low compared to axial forces. Furthermore, this method necessitates modifications to the bolt, the impact of which on its primary function must be carefully evaluated. The lack of temperature compensation was again noticeable here.

The third iteration incorporates temperature compensation and accounts for distinct sensitivities to axial and bending loads.

This sensor design is published in more detail under [45] and [46]. The optimal parameter set describing the available design space set inside the bolt is $r_1 = 8.2\,\text{mm}$, $h_1 = 6.4\,\text{mm}$, $r_2 = 6\,\text{mm}$, and $h_2 = 20\,\text{mm}$ (Fig. 7). This configuration results in a relative bolt resilience of 76.5%, which is roughly equivalent to one strength class and is

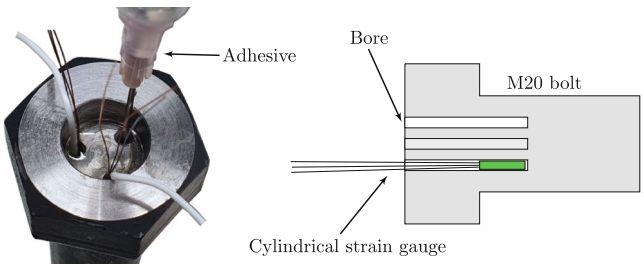

Fig. 5 Each cylindrical strain gauge is inserted in a 2 mm bore without further alignment. The remaining bore volume is then filled using a PTFE tube and adhesive provided by the strain gauge manufacturer (EP70, HBK, Darmstadt, Germany)

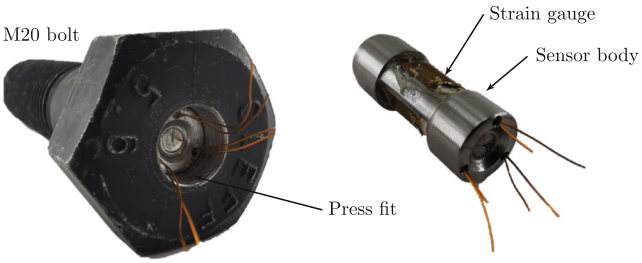

Fig. 6 Three strain gauges are applied to a cylindrical sensor body and then into the bolt, enabling alignment of each strain gauge with more precision

therefore compensated by using a bolt of a higher strength class to machine the cavities. The strength of a class 5.8 bolt with added cavities corresponds to a conventional bolt of strength class 5.6.

Simultaneously measuring the axial force F_z and the two bending torques M_x and M_y requires three decoupled output signals with minimal cross-talk. The working range of standardized bolts requires different measurement ranges for the axial and bending forces due to the bolts pretension in axial direction. Therefore, the sensor is designed using bending beams and the compensation effects of a half-bridge configuration detailed in [45] with different sensitivities for axial and bending forces.

The force sensor is based on a deformation body, whose purpose is to deform in a controlled manner such that measurements at specific locations establish a linear relationship with the applied forces. The geometry of the body is designed to facilitate precise alignment of the individual strain gauges, addressing alignment issues identified in the initial prototypes. The sensor design incorporates three vertical bending beams arranged symmetrically around the bolt's central axis (Fig. 7). Due to their off-center placement, both axial and bending forces introduced to the sensor induce bending in the beams with different magnitudes. Bending torques introduced to the sensor lead to larger bending of each beam than axial forces, which are only levered through the off-centered position.

In preliminary tests, various custom and commercial resistive and piezoresistive sensing principles were evaluated regarding their applicability to the specific application and compared to the commercially available cylindrical bolt strain gauges for axial force measurements. Foil strain gauges were selected for this sensor due to their commercial availability, compact size, linear response, and compatibility with the chosen deformation body geometry. Each bending beam is equipped with two strain gauges, resulting in a total of six strain gauges in the sensor, able to compensate temperature influences. The strain gauges are positioned on the inner and outer surfaces of the beams. Opposing elongation and compression of these surfaces results in a differential change in the bridge output. Uniform strain variations as well as temperature induced equal changes are inherently compensated by the bridge configuration. The bridge output signal is measured as a ratio of the excitation voltage and expressed in mV/V. Current consumption can be kept low by using strain gauges with high basic resistances.

The exact strain gauge positions were determined extending the finite element simulation conducted with COMSOL Multiphysics 5.6 (COMSOL AB, Stockholm, SWE) already used to determine the design space parameters. Due to the complex geometry, the sensor body is manufactured externally and subsequently integrated into the bolt using a threaded connection at the top (M12 × 0.75) and adhesive bonding on the bottom surface (Araldite® 2014-2, Huntsman Advanced Materials GmbH, Basel, CHE).

3.2 Sensor characterization

Characterization of the sensor outside the bolt was carried out using a custom measurement setup in a universal testing-machine (type: inspekt Table5, Hegewald & Peschke, Nossen, DE) equipped with a reference force sensor (type: 1000 N S2M with 0.02% accuracy, HBK, Darmstadt, DE)

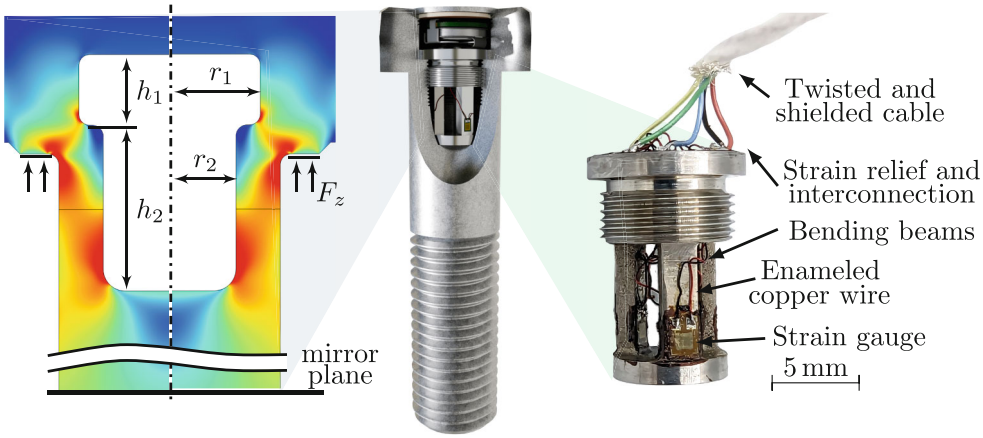

Fig. 7 The design space determined from simulations under axial loads F_z results in a remaining load capacity of 76.5%. The sensor, consisting of three vertical bending beams, is optimized to measure both axial and bending loads within this space

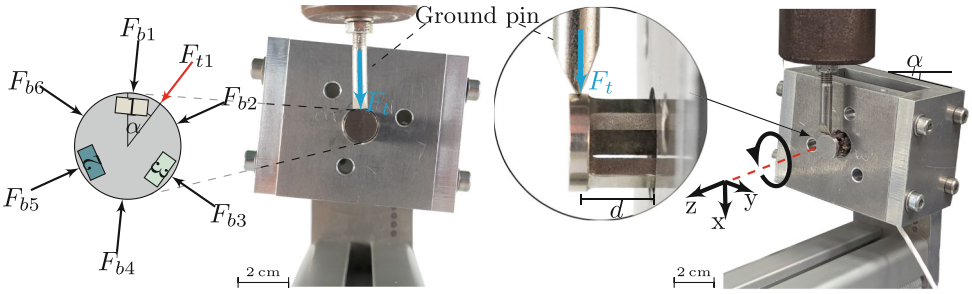

Fig. 8 A custom test fixture is utilized to apply bending loads from multiple directions within a testing machine. The force F_t is introduced in a controlled and localized manner using a ground pin with a V-shaped edge, which makes tangential contact with the curved surface. The applied force from the testing machine F_t is mapped to the sensor's coordinate system based on the introduction angle α and the bending length d. Reproduced, with permission, from [46]. Copyright 2024 IEEE

(Fig. 8). This allows for shorter development cycles for the sensor itself and to assess which errors are caused by the sensor itself and which are caused by subsequent integration. The developed sensor exhibits a small linearity error of ±0.82% for axial load and ±0.11% for bending load. The hysteresis error is ±1.53% for axial load and ±0.52% for bending load (Fig. 9). The decoupling matrix was derived from recorded data pairs consisting of known reference forces and corresponding sensor signals using the least-squares regression method. This matrix enables the computation of the acting loads on the sensor from the measured signals. For validation, a subset of the measured data was excluded from the matrix derivation, allowing an assessment of its accuracy. For combined (multiaxial) load, the decoupling error is 2.5%.

3.3 Integration in the bolt

In the next step, the sensor was integrated into an M20 bolt of strength class 5.6 with a length of 150 mm, creating a functional prototype of a bolt with a multiaxial force measurement. The required cavities are machined into the bolt, including the M12 × 0.75 thread used to mount the sensor. For quantitative evaluation of the installation, the bolt is loaded axially in a different testing machine(type: AllroundLine Z100, ZwickRoell GmbH & Co. KG, DE) with a 100 kN reference force sensor (type: XfoceK with 0.02% accuracy, ZwickRoell GmbH & Co. KG, DE) with a nominal force of 10 kN. The linearity error of ±1.01% is comparable to the sensor's linearity and demonstrates the successful strain transfer from the bolt to the sensor.

In the same setup, the sensor bolt's ability to detect small lateral forces under axial preload was demonstrated by applying lateral loads of approximately 10 N from various directions with a finger (Fig. 10). Although the bending torques are small relative to the operational range of an M20 bolt, the sensor accurately detects the direction of bending with high sensitivity. This experiment also showcases the successful implementation of distinct working ranges and sensitivities for both axial and bending forces within the sensor. In the next step, electronics are integrated in the second cavity.

4 Electronics

This section introduces a modular strain gauge readout platform aimed at overcoming sensor integration challenges from an electronics standpoint. The platform is intended as a testing framework for evaluating various energy supply and communication strategies. Special focus is placed on the development and evaluation of the multichannel strain gauge readout electronics, prioritizing energy efficiency per data point while also addressing temperature compensation.

4.1 Electronics system design

The electronics are constrained to fit within the calculated maximum cavity (Section 2) 12 mm diameter and 6 mm height. Both the electronics and energy storage needed to be integrated within this limited volume. A folded and stacked printed circuit board (PCB) design was implemented (Fig. 12 and 13), to optimize space utilization while ensuring manufacturability and ease of assembly. The electronic platform is based on a 100 mm thick flexible PCB with two 17.5 mm rolled copper layers, allowing a one-time flexing radius of 1 mm. This design enables the integration of up to four stacked layers within the bolt (Fig. 12 and 13). As illustrated in Fig. 12, the electronics platform consists of two modules: a flexible PCB carrying the precision measurement circuitry and a rigid multilayer PCB containing the power supply and communication module. This modular approach minimizes design risk and facilitates the evaluation of various power supply and communication concepts. For streamlined assembly, one end of the flexible PCB is glued to the deformation body (Fig. 11), providing both soldering pads and mechanical relief for the strain gauge wires. Using an assembly tongue, the defor-

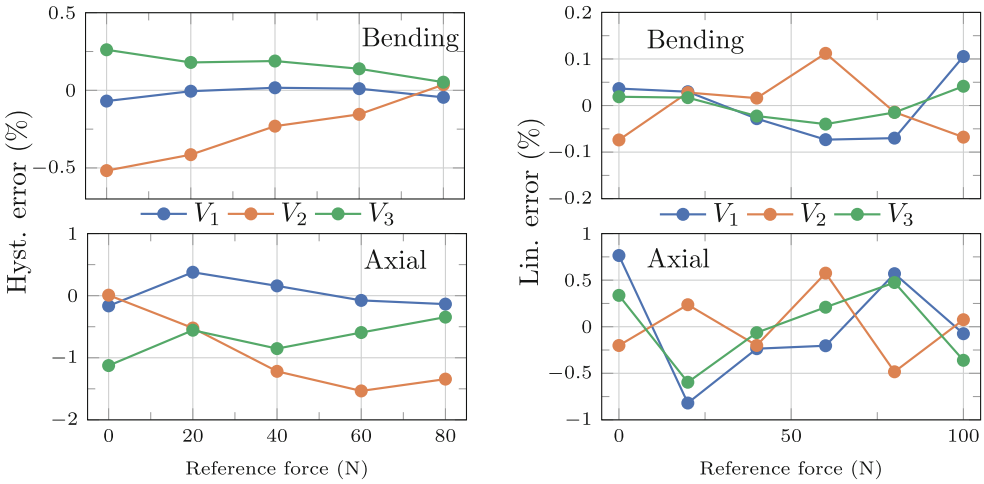

Fig. 9 Hysteresis and linearity errors of the three half-bridge output signals for bending and axial load cases of the presented multi-axial sensor. The linearity error represents the deviation between the best-fit line and the measured values, expressed as a percentage of the nominal load. In contrast, the hysteresis error describes the difference in measurements for the same load during the loading and unloading cycles of the sensor

mation body can be screwed into the bolt with the pre-assembled electronic module attached. In the final step, the flexible PCB is carefully folded into the cavity. To ensure reliable connectivity between the different modules, the communication and energy supply module is linked to the flexible base PCB using stacked PCB technology (Fig. 12). This approach allows the use of high-layer-count PCBs with tight tolerances for digital electronics while enabling cost-effective and rapid module iterations—a significant advantage over direct rigid-flex PCB designs.

4.2 Energy supply and harvesting concepts

Various energy harvesting and transmission concepts were investigated, focusing on solutions compatible with a base station to maximize versatility. Specifically, high-frequency rectifiers, inductive charging, photovoltaic, and energy transmission via body ultrasound were evaluated as potential energy sources. Among these, energy harvesting at 868 MHz and 2.4 GHz using a high-frequency rectifier circuit and a sufficiently large antenna proved feasible (Fig. 14a). However, the received power is significantly limited due to transmission losses and regulatory constraints on radiation power. Inductive energy transfer via commercial Near Field Communication (NFC) [48] integrated circuit (IC) achieved power levels up to 50 mW. To integrate this technology into the bolt, a dedicated antenna was developed based on a flexible PCB with ferrite foil to minimize iron losses (Fig. 14b). Photovoltaic energy harvesting was evaluated using two small solar cells mounted on the screw head (Fig. 14c). Under an illumination intensity of 100 mW/cm², simulating direct sunlight, up to 100 mW of power could be harvested. Even under indoor lighting conditions of 500 lx, over 500 µW remained harvestable, making photovoltaic suitable for well-lit environments or outdoor applications. Additionally, energy transmission via body ultrasound was explored, demonstrating a fundamental proof of concept using two piezoelectric crystals clamped onto a steel plate (Fig. 14d). This approach enabled both energy and data transfer, presenting a promising method for fully encapsulated electronics. For the first prototype, a standard CR1220 35 mA h primary battery

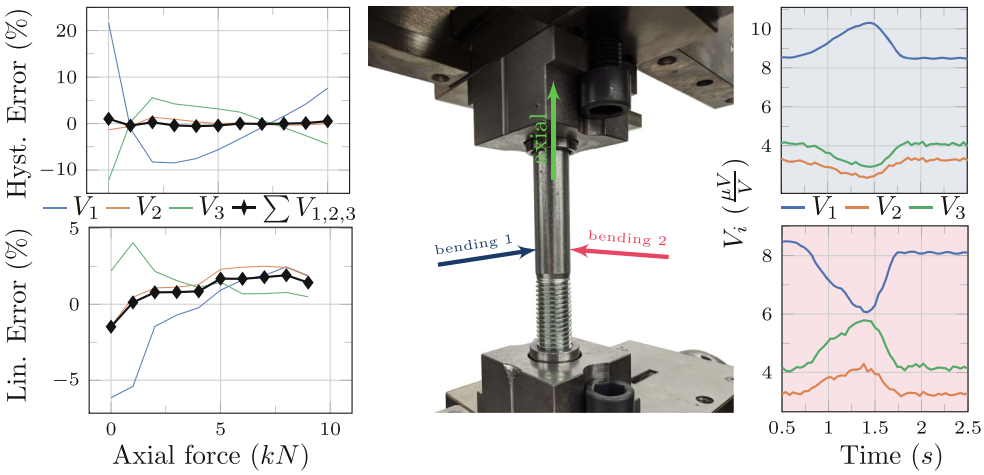

Fig. 10 First, the bolt is axially preloaded with 10 kN while measuring the bridge output signals V_i relative to the supply voltage. The linearity error of the individual signals is large at low loads but remains low in the summed signal, effectively compensating for bending influences as predicted by analytical considerations. The hysteresis error for the sensor-bolt is higher than for the sensor alone. Second, a finger is used to introduce additional bending moments from different directions (blue and red) transversely

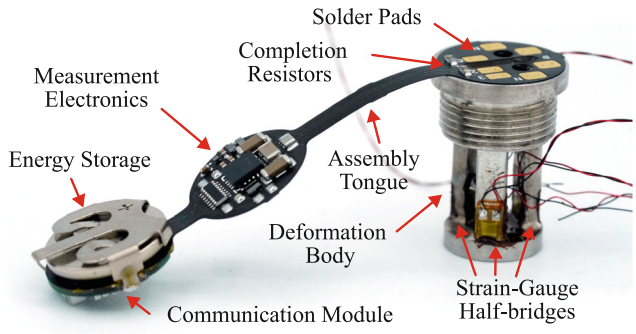

Fig. 11 Flexible strain-gauge readout platform glued to the deformation body [45, 46] during assembly before soldering. Reproduced, with permission, from [47]

was selected. However, the current version integrates an enerCera ET1210C-H 4 mW h rechargeable cell (NGK Insulators LTD., Nagoya, Japan), which supports operating temperatures up to 105 °C, overcoming common limitations of lithium-ion technology [49]. The battery voltage is either boosted to 3.3 V or passed through when higher, using a TPS61299 boost converter (Texas Instruments, Dallas, USA), ensuring operation down to 1 V and maximizing energy utilization (Fig. 15). The regulated 3.3 V supplies both the microcontroller and a low-noise low-drop-out regulator (LDO) for the analog circuit. The modular design allows application-specific energy supply concepts to be integrated, including NFC charging, radio frequency (RF) harvesting, and ultrasonic charging. Notably, ultrasonic charging provides a unique advantage: the ability to fully encapsulate the sensor and electronics within metal, ensuring complete water and gas tightness [36, 50, 51].

4.3 Communication

The modular platform enables flexible adaptation of the communication protocol based on the specific use case and distance to the base station. Three approaches were selected for further development: NFC for short distances, Bluetooth Low Energy (BLE) for high data rates over medium distances, and Long Range Wide Area Network (LoRaWAN) for long-range transmission. For the initial prototype, a battery-powered BLE solution was implemented using the BGM220 microcontroller (Silicon Labs, Austin, USA). This setup supports either continuous data transmission or advertisement-based failure notifications in case of SiMe malfunction. To minimize energy consumption, deep sleep features were utilized, reducing the total system current to approximately $I_{\mathbf{Sleep}} \approx 500nA$, with wake-up capability triggered by an 2.4 GHz on-off keying (OOK) signal or a periodic timer. The BLE implementation is based on Bluetooth 5.2, with Bluetooth 5.4 and its Periodic Advertising with Responses (PAwR) feature being a promising upgrade for future revisions to ensure reliable reception of advertisements [53]. To extend communication range, a 868 MHz LoRa module is under development, targeting improved performance in metallic environments [54–56]. Additionally, NFC-based prototypes were evaluated for short-range communication and energy transfer, leveraging an optimized antenna design on a flexible PCB (Fig. 14b).

4.3.1 Antenna integration

Integrating antennas within the SiMe presents significant challenges due to space constraints and the surrounding metallic environment. To prevent electromagnetic shielding, a designated non-conductive window is incorporated into the metallic housing, as recommended in [33, 34, 57]. The internal antenna of the BGM220 combined with a PCB loop was deemed unsuitable due to space limitations. Instead, the final BLE prototype utilizes a compact $5 \times 2 \times 1.5\text{mm}^3$ chip antenna, optimized for on-metal integration and sufficient performance within the bolt head (Fig. 12). For longer transmission distances at 2.4 GHz, a patch antenna prototype was developed, as shown in Fig. 14a. In addition to data transmission, electromagnetic energy harvesting requires careful antenna design due to strict transmission power limitations. For short distances, inductive methods such as NFC offer a viable alternative [32–34]. Figure 14b shows the developed NFC antenna, which can be seamlessly integrated into the modular platform. It is optimized for power transfer based on a flex PCB and a WE-FSFS 364 ferrite foil (Würth Elektronik eiSos GmbH & Co. KG, Waldenburg, DE) for minimizing eddy current losses in the bolt steel.

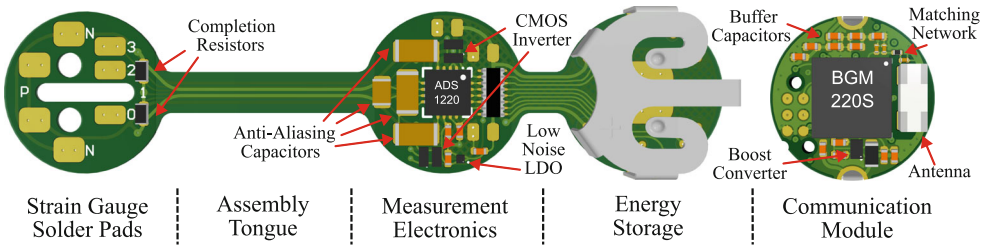

Fig. 12 Proposed flexible modular electronics platform, divided into sub-modules, with an interchangeable communication/power supply module for adaptation of the platform to different use case scenarios. Reproduced, with permission, from [47]

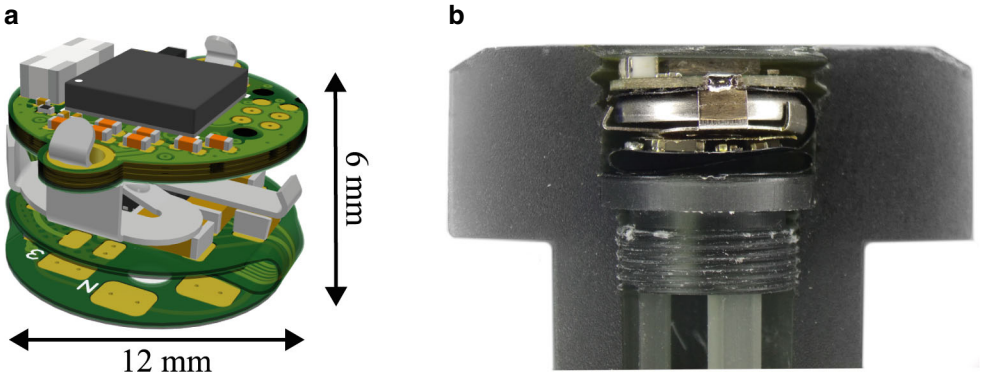

Fig. 13 Folded stack up of the proposed electronics platform (**a**) and integration in the cross section of a M20 bolt (**b**)

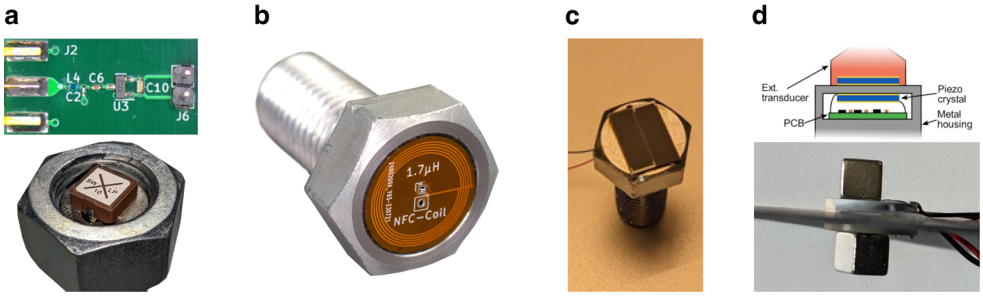

Fig. 14 Evaluation of energy transmission and harvesting concepts, based on RF-harvesting (**a**), inductive coupling (**b**), photovoltaic (**c**) and solid body ultrasound (**d**)

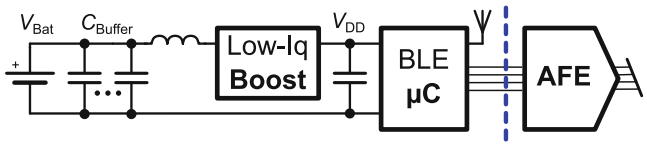

Fig. 15 Reduced schematic of the BLE communication and power supply module with buffer capacitors for stabilizing the battery voltage and a boost regulator to allow operation down to $V_{Bat} > 1V$. Reproduced, with permission, from [52]

4.3.2 Data processing and energy optimization

Since the power consumption of the transmission electronics directly affects device longevity, various preprocessing and compression techniques were considered. The sensor node internally processes measured voltage values using a 3×3 calibration matrix, converting them into force values. Each resulting data point consists of three force values in IEEE754 32-bit float format and one temperature reading in 16-bit integer format, totaling 112 bytes, making compression for transmission over BLE unnecessary. In cases where data is stored in non-volatile memory or transmitted using a slower communication protocol, the 32-bit floating point strain values can be reduced to 16-bit integers, and delta compression can be applied to optimize storage and transmission efficiency. To further reduce power consumption, an adaptive transmission strategy can be implemented for critical monitoring applications. Instead of continuously transmitting measurement data, the system can send periodic alive pings, with the absence of these pings being interpreted as a failure condition. This significantly reduces transmission energy while maintaining system reliability.

4.4 Strain gauge evaluation

The primary factors influencing energy consumption were identified as the strain gauge evaluation and data transmission from the SiMe. Since the energy demand of the strain gauge is strongly dependent on its base resistance, different resistance values were analyzed by comparing the signal-to-noise ratio (SNR) against power consumption. Based on these evaluations, a 1 kΩ strain gauge was selected as the optimal choice due to its lower power requirements (Section 3). A voltage-based measurement approach using a commercially available analog front-end and 24-bit analog to digital converter (ADC) ADS1220 (Texas Instruments, Dallas, USA) was chosen. While time-based measurement techniques were also considered, they were ultimately discarded due to the lack of commercially available hardware. At the core of the measurement circuit is the provision of a stable, low-noise supply voltage for both the strain gauge and the analog electronics. The anti-aliasing filters at the input were optimized to balance settling time and noise performance, ensuring a total measurement time of 3.3 ms for acquiring temperature data and three half-bridge voltages (Fig. 16; [47]).

The developed circuit (Fig. 17 and 12) was evaluated using a strain gauge simulator (Fig. 18) and tested under controlled conditions in a climate chamber. During these tests, an offset drift was observed, prompting a refinement

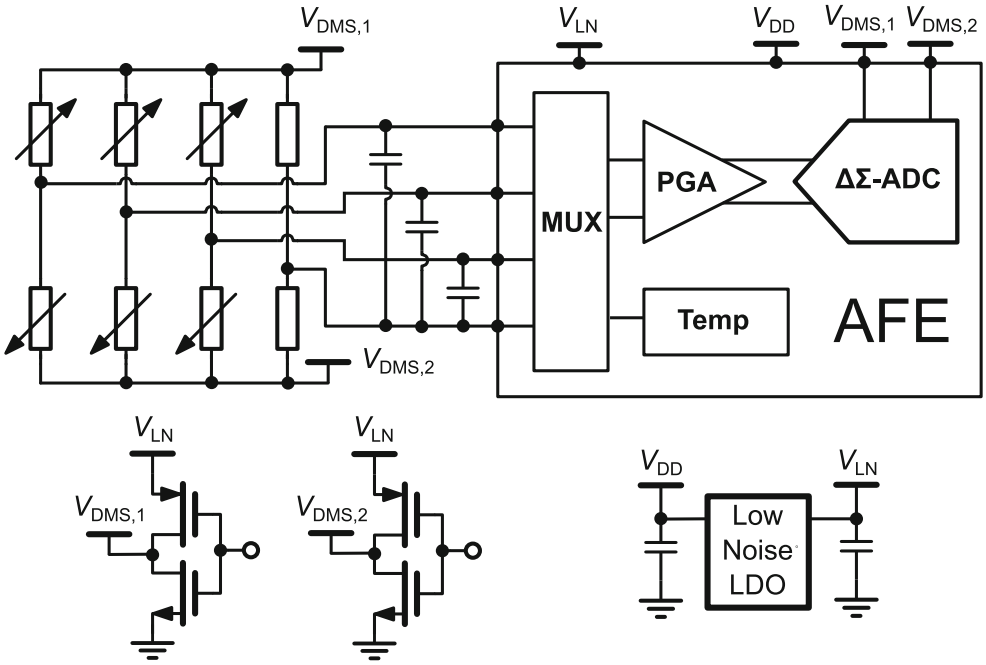

Fig. 16 Current consumption of the strain gauge readout circuit for measuring one datapoint without offset compensation. In total 13.95 µC · 3.3 V = 46.04 µJ energy is required. Reproduced, with permission, from [47]

in the next design iteration: the supply current was made reversible using two discrete complementary metal-oxide-semiconductor (CMOS) inverters, effectively compensating for temperature-induced offset voltages in the measurement signal (Fig. 19; [47]).

5 Methodical development of sensor integrating bolts

A problem in the development of sensor integrating machine elements is the integration of sensing functions while maintaining mechanical functions. Especially the case of integrating novel sensory functions into an already fully developed and standardized machine element like a bolt is a huge challenge. This leads to a conflict of objectives between a high performance of the machine element (mechanical function) and high-quality sensor data (electrical domain). There is a lack of methodical approaches for sensor integration into machine elements that encompasses solving this conflict. Therefore, a methodology was extracted out of this project to support engineers to overcome this conflict by methodically supporting the design of sensing functions into machine elements using the example of bolts [58].

This method focuses on the initial three objectives mentioned in the introduction:

1. identification of an optimal design space for sensors,
2. design of a deformation body for multiaxial force measurement and
3. integration of the electronics to acquire and transfer measurement data.

The first part focuses on the identification of the design space. This is of crucial importance, as it significantly affects the fulfillment of both mechanical and sensory functions, as highlighted in the project [26]. For this purpose, a method was developed to systematically optimize the design space of an M20 bolt [41]. The method is applied

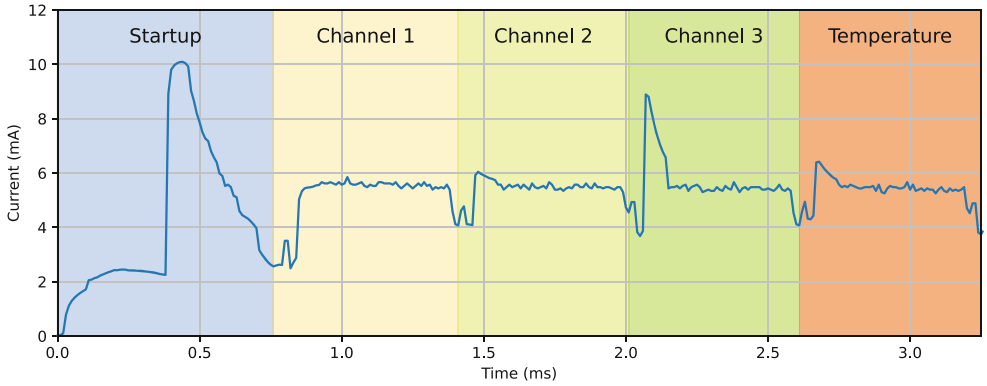

Fig. 17 Reduced schematic of the strain gauge readout circuit with CMOS inverter for offset compensation and minimizing the on-time of the strain gauges. Reproduced, with permission, from [47]

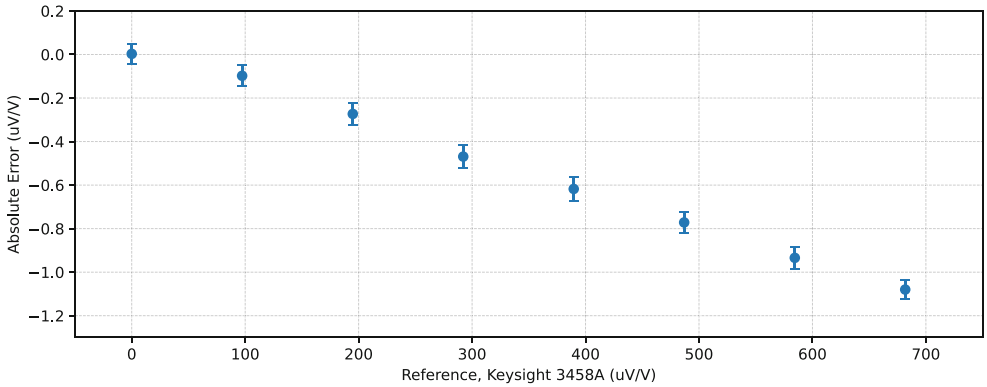

Fig. 18 Gain error of the readout circuit under controlled temperature conditions. The absolute error is less than 1.2 µV/V and the relative error is below 0.2%. Reproduced, with permission, from [47]

to the machine elements of two other subprojects of the SPP2305, "Microelectronic modular system for sensor-integrating machine elements" (Prof. Kirchner, Prof. Krause, Prof. Trieu; Pr. No. 466493340) and "Elastic couplings with integrated flexible dielectric elastomer sensors" (Dr. Henke, Prof. Schlecht, Prof. Wallmersperger; Pr. No. 466661922), in order to assess the transferability and promote synergies within the SPP2305 [44].

The second and third part focus on the design of the sensor and the electronics, which have been outlined in detail in the previous chapters.

All of the three parts are combined in a framework (Fig. 20), which is based on VDI 2206 (V-model) and the methodology of testing, published in [58]. The V-model is suitable as it best reflects the procedure in the project. A workshop on the methodological approach and testing held in a SPP2305 working group showed that a similar approach was used profitably in most of the subprojects in the SPP2305. The methodology of testing is integrated to use its support in acquiring missing design knowledge to synthesize embodiment solutions.

The process's strength lies in leveraging existing information about bolts and force sensors, allowing the use of analytical equations and models to gain knowledge about mechanical and sensory functions. This approach is transferable to other sensor-integrating machine elements.

Another strength is the early and iterative virtual and physical check of embodiment solutions, which helps identify and resolve conflicts of objectives early, especially in domain interactions. Most failed checks in the case study were due to unforeseen dependencies, highlighting the likelihood of domain conflicts when integrating sensors into existing machine elements. A negotiation model is used to acquire knowledge about these interactions.

Additionally, the sequence of empirical testing is crucial due to its cost implications. Premature testing is expensive due to a large solution space, while late testing incurs high iteration costs. The first empirical test followed literature research and analytical/model-based testing, narrowing the solution space and keeping costs low. Empirical tests should be conducted only when the solution space is sufficiently small to avoid high costs [58].

6 Conclusion and outlook

Despite the existence of force measuring bolts in the state of the art, they exhibit distinct disadvantages in measuring all pertinent load cases, impairing the mechanical function, altering the mechanical interfaces, and managing energy. During the initial funding period (FP 1), the project successfully investigated a sensor integrating bolt (SiS, Fig. 21) that is able to measure axial forces and bending torques

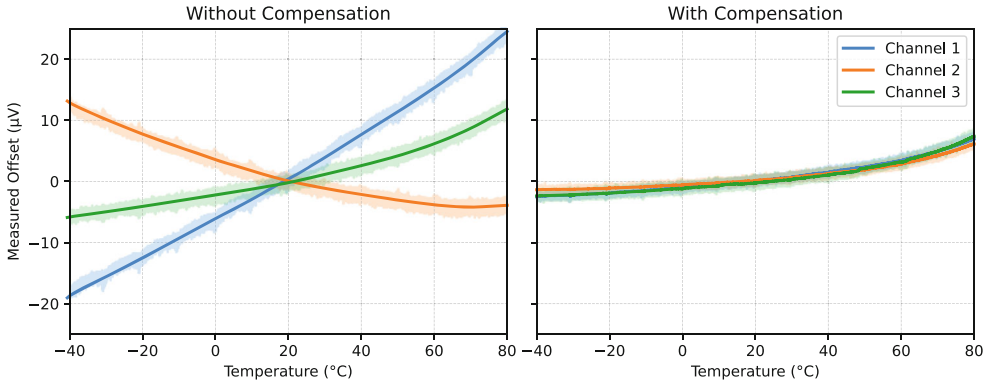

Fig. 19 Measured offset voltage over a range of –40 °C to 80 °C. With compensation the temperature dependent offset drift is reduced from 1 µV/K to 0.1 µV/K. Reproduced, with permission, from [47]

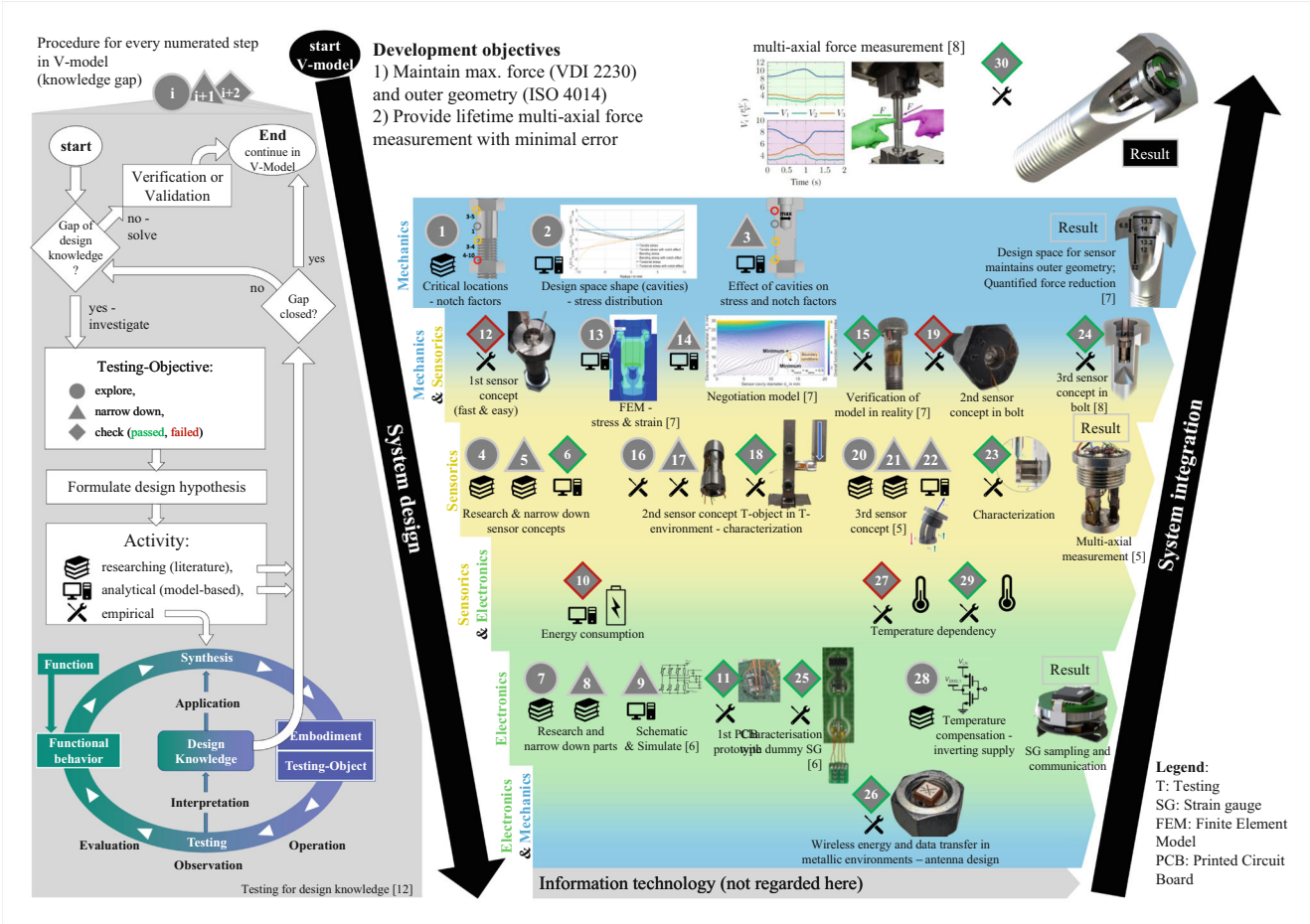

Fig. 20 Combination of V-model and method of testing to gain missing knowledge in the development of the sensor integrating bolt. The left-hand side shows the procedure for each step where missing knowledge needs to be acquired. The right-hand side shows the V-model with all enumerated steps where knowledge was acquired throughout the development. The figure is based on [58]

with independent sensitivities while integrating all sensor and electronic parts needed to measure and communicate the data inside the bolt. Thus, the standardized interfaces are maintained. The project's findings revealed an optimal design space for the sensor, which fulfills mechanical and sensory functions under the given boundary conditions of assembly and mechanical stress increase [41, 42]. With regard to the following funding period, the proof of reliability and lifetime determination remains to be substantiated.

The strain gauge-based sensor concept has been demonstrated to measure and decouple the relevant loads of a bolt tightened in accordance with VDI 2230. The accuracy of the measurement concept in the bolt, in the form of linearity and hysteresis errors, was determined to be ±1.01% and 6.15%, respectively, [45, 46]. Further research will enhance our understanding of the measurement's reliability, its performance over the service life, and the effect of tightening on it.

The energy and data transmission electronics boast a modular design, allowing for adaptation depending on the installation situation [52]. This enables the use of synergies in other sensor integrating projects like the SPP2305. A range of approaches, including cable-, solar-, HF (BLE, LoRa), NFC- and ultrasonic-based methods, have been implemented and tested. The energy consumption per measurement of a data point was reduced to 46 µJ, representing a significant reduction in energy usage. The electronics implemented on a flexible printed circuit board enable easy installation in the bolt. Further investigation is needed to explore the behavior of radio-based energy and data transmission concepts (HF, NFC) in particular in closed metallic environments and the effect on the achievable performance. Through-metal acoustic energy transfer, a novel method in this area, achieved promising results in initial preliminary tests as part of funding period 1, and is to be investigated in greater detail in the future.

The function of each bolt connection is greatly influenced by the assembly process. The novel SiS promises to enhance the precision of bolt tightening in combination with standard tightening methods compared to conventional

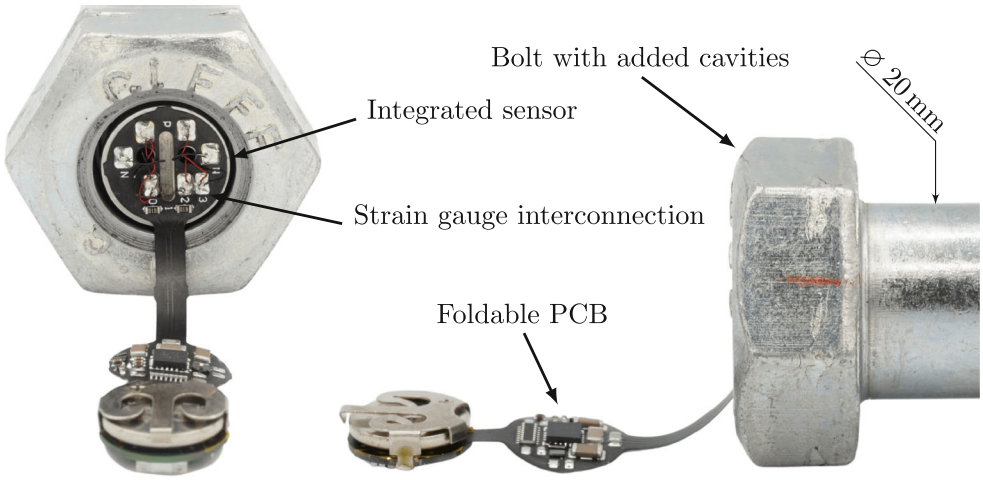

Fig. 21 The design space optimization results, the sensor developed for this purpose, and the modular electronics for evaluation are integrated into a complete prototype

bolts that are tightened via torque. Additionally, the method extracted out of the project can support the development of cylindrical sensor-integrating machine elements for supporting future developers and sensor integration projects. The method is based on the bolt example and adheres to the principles outlined in VDI 2206 and the testing methodology, combining their strengths. A part of the design space optimization method was used in other sub projects of the priority program SPP2305.

All in all, the novel sensor integrating bolt can be used to measure axial and bending loads on bolts and to indicate early failure like decrease of clamping force or opening joints. The method can be used to support future sensor integration projects.

Acknowledgements On behalf of all authors, the corresponding author states that there is no conflict of interest.

Funding This work was funded by the Deutsche Forschungsgemeinschaft (DFG, German Research Foundation)—466650813 within SPP2305—441853410

Author Contribution David Riehl und Julian Peters contributed equally to this work. Author CRediT roles: Conceptualization, methodology, data curation, formal analysis, investigation, visualization, validation: D.R., D.L. (electronics) J.P. (Design methodology, sensor 1st versions), F.H. (sensor final versions); writing original draft preparation, D.R., J.P., F.H., D.L.; writing—review and editing, D.R., J.P., K.H., S.M., M.K.; supervision, project administration, funding acquisition, resources: K.H., S.M., M.K.

Funding Open Access funding enabled and organized by Projekt DEAL.

References

1. Kalsoom T, Ramzan N, Ahmed S, Ur-Rehman M (2020) Advances in sensor technologies in the era of smart factory and industry 4.0. Sensors. https://doi.org/10.3390/s20236783
2. Bian Q, Bauer C, Stadler A, Lindner M, Jakobi M, Volk W, Koch AW, Roths J (2021) In-situ high temperature and large strain monitoring during a copper casting process based on regenerated fiber Bragg grating sensors. J Lightwave Technol 39(20):6660–6669. https://doi.org/10.1109/JLT.2021.3101524
3. Kirchner E, Martin G, Vogel S (2018) Sensor integrating machine elements: key to in-situ measurements in mechanical engineering. In: Schützer K (ed) 23° Seminário Internacional de Alta Tecnologia
4. Groche P, Hohmann J, Übelacker D (2019) Overview and comparison of different sensor positions and measuring methods for the process force measurement in stamping operations. Measurement 135:122–130. https://doi.org/10.1016/j.measurement.2018.11.058
5. Hofmann K, Keil F, Matthiesen S, Gwosch T, Kupnik M, Kirchner E, Göhringer D, Otto M, Stahl K (2022) Potenziale und Herausforderungen Energieautonomer Sensorsysteme für den Einsatz in sensorintegrierenden Maschinenelementen. EASS 2022: Energieautonome Sensorsysteme, vol 102. VDE, Berlin, pp 36–38 (GMM-Fachbericht)
6. Kirchner E, Wallmersperger T, Gwosch T, Menning JDM, Peters J, Breimann R, Kraus B, Welzbacher P, Küchenhof J, Krause D, Knoll E, Otto M, Muhammedi B, Seltmann S, Hasse A, Schäfer G, Lohrengel A, Thielen S, Stiemcke Y, Koch O, Ewert A, Rosenlöcher T, Schlecht B, Prokopchuk A, Henke E-FM, Herbst F, Matthiesen S, Riehl D, Keil F, Hofmann K, Pape F, Konopka D, Poll G, Steppeler T, Ottermann R, Dencker F, Wurz MC, Puchtler S, Baszenski T, Winnertz M, Jacobs G, Lehmann B, Stahl K (2024) A review on sensor-integrating machine elements. Adv Sens Res. https://doi.org/10.1002/adsr.202300113
7. Hendrich N, Wasserfall F, Zhang J (2020) 3D printed low-cost force-torque sensors. IEEE Access 8:140569–140585. https://doi.org/10.1109/ACCESS.2020.3007565

8. Vorwerk-Handing G, Gwosch T, Schork S, Kirchner E, Matthiesen S (2020) Classification and examples of next generation machine elements. Forsch Ingenieurwes 84(1):21–32. https://doi.org/10.1007/s10010-019-00382-1
9. (2020) DFG Schwerpunktprogramm 2305: Sensorintegrierende Maschinenelemente: Wegbereiter der flächendeckenden Digitalisierung. https://www.spp2305.de/. Accessed 1 Aug 2025
10. Groche P, Brenneis M (2014) Manufacturing and use of novel sensoric fasteners for monitoring forming processes. Measurement 53:136–144. https://doi.org/10.1016/j.measurement.2014.03.042
11. (1999) DIN 13-1: ISO general purpose metric screw threads—Part 1: Nominal sizes for coarse pitch threads; nominal diameter from 1 mm to 68 mm. https://doi.org/10.31030/8133800
12. DIN EN ISO 4014:2022-10, Verbindungselemente – Sechskantschrauben mit Schaft – Produktklassen_A und_B (ISO_4014:2022); Deutsche Fassung EN_ISO_4014:2022. Beuth Verlag GmbH, Berlin. https://doi.org/10.31030/3279821
13. VDI 2230 Blatt 1: 2015-11: Systematische Berechnung hochbeanspruchter Schraubenverbindungen: Zylindrische Einschraubenverbindungen, Berlin (2015)
14. Blachowski B, Gutkowski W (2016) Effect of damaged circular flange-bolted connections on behaviour of tall towers, modelled by multilevel substructuring. Eng Struct 111:93–103. https://doi.org/10.1016/j.engstruct.2015.12.018
15. Templeman JO, Sheil BB, Sun T (2020) Multi-axis force sensors: a state-of-the-art review. Sensors Actuators A: Phys 304:111772. https://doi.org/10.1016/j.sna.2019.111772
16. Frank T, Grün A, Kermann M, Cyriax A, Steinke A, Ortlepp T, Reschke G (2019) 2.2.4 Hybridintegration von Mikrodehnungssensoren. In: 20. GMA/ITG-Fachtagung Sensoren und Messsysteme 2019. AMA, Nuernberg, pp 153–158 https://doi.org/10.5162/sensoren2019/2.2.4
17. Biehl S, Paetsch N, Meyer-Kornblum E, Bräuer G (2016) Wear resistenat thin film sensor system for industrial applications. Int J Instrum Meas (1):6–11
18. IST, F.: Intelligente Schraubverbindung – Drahtlose und energieautarke Monitoringlösung. https://www.ist.fraunhofer.de/de/referenzprojekte/intelligente-schraubverbindung.html. Accessed 25 July 2022
19. Brenneis M, Groche P (2014) Integration of Piezoceramic tube under prestress into a load carrying structure. AMR 966–967:651–658. https://doi.org/10.4028/www.scientific.net
20. ConSenses. https://consenses.de/en/products/sensors/force-and-vibrationsensors. Accessed 16 Oct 2025
21. Core Sensing Datasheet CoreIN. https://core-sensing.de/app/uploads/2022/12/coreIN-core-sensing.pdf. Accessed 2 Mar 2023
22. Sensorise Sensorise SmartScrew. https://sensorise.de/solutions/smartscrew/. Accessed 25 Apr 2023
23. VALLEY FORGE and BOLT: SPC4 Load indicating system Product Information. https://www.vfbolts.com/product/spc4-load-indicating-system-2/. Accessed 29 Nov 2023
24. Intellifast Intellifast System—Intellifast. https://www.intellifast.de/intellifast-system/ (Created 7 Mar 2024). Accessed 7 Mar 2024
25. Horn S, Gwosch T, Matthiesen S (2021) Sensor-integrated chemical anchor for continuous monitoring of the fastening situation. Beton Stahlbetonbau. https://doi.org/10.1002/best.202000105
26. Peters J, Zimmerer C, Gwosch T, Herbst F, Hartmann C, Chadda R, Riehl D, Keil F, Kupnik M, Hofmann K (2022) Test-driven development to overcome challenges in the design of sensor-integrating machine elements. In: DS 119: proceedings of the 33rd Symposium Design for X (DFX2022). The Design Society, Hamburg, p 10 https://doi.org/10.35199/dfx2022.12
27. Olsson RH, Bogoslovov RB, Gordon C (2016) Event driven persistent sensing: overcoming the energy and lifetime limitations in unattended wireless sensors. In: 2016 IEEE SENSORS. IEEE, Orlando, pp 1–3 https://doi.org/10.1109/ICSENS.2016.7808398
28. Wang P-HP, Jiang H, Gao L, Sen P, Kim Y-H, Rebeiz GM, Mercier PP, Hall DA (2018) A near-zero-power wake-up receiver achieving –69-dBm sensitivity. IEEE J Solid-State Circuits 53(6):1640–1652. https://doi.org/10.1109/JSSC.2018.2815658
29. Viehweger C, Keutel T, Kasper L, Pfeifer T, Kanoun O (2013) System design and energy management for indoor solar energy harvesting under consideration of spectral characteristics of solar cells. Int J Meas Technol Instrum Eng 3(1):1–15. https://doi.org/10.4018/ijmtie.2013010101
30. Naifar S, Bradai S, Kanoun O (2022) Design study of a nonlinear electromagnetic converter using magnetic spring. Eur Phys J Spec Top 231(8):1517–1528. https://doi.org/10.1140/epjs/s11734-022-00498-6
31. Talla V, Kellogg B, Ransford B, Naderiparizi S, Smith JR, Gollakota S (2017) Powering the next Billion devices with wi-fi. Commun ACM 60(3):83–91. https://doi.org/10.1145/3041059
32. Trautmann M, Sanftl B, Weigel R, Koelpin A (2019) Simultaneous inductive power and data transmission system for smart applications. IEEE Circuits Syst Mag 19(3):23–33. https://doi.org/10.1109/MCAS.2019.2924508
33. Riehl D, Herold M, Keil F, Hofmann K (2022) Discrete low-cost implementation of inductive energy and data transmission for deeply integrated sensor systems. In: EASS 2022: Energieautonome Sensorsysteme. GMM-Fachbericht, vol 102. VDE, Berlin Offenbach, pp 53–55 (https://ieeexplore.ieee.org/document/9899266)
34. Finkenzeller K (2008) RFID-Handbuch: Grundlagen und Praktische Anwendungen Von Transpondern, Kontaktlosen Chipkarten und NFC, 5th edn. Hanser, München https://doi.org/10.1002/9780470665121
35. Tang X, Mandal S, Ozdemir T (2022) A CMOS SoC for wireless ultrasonic power/data transfer and SHM measurements on structures. IEEE Access 10:110163–110180. https://doi.org/10.1109/ACCESS.2022.3214231
36. Korner D, Riehl D, Hofmann K (2023) Ultrasonic energy harvesting and communication asic for sensor-integrated machine elements. In: MikroSystemTechnik Kongress, pp 734–738 (https://ieeexplore.ieee.org/document/10483118)
37. Magrin D, Capuzzo M, Zanella A, Vangelista L, Zorzi M (2021) Performance analysis of loRaWAN in industrial scenarios. IEEE Trans Ind Informatics 17(9):6241–6250. https://doi.org/10.1109/TII.2020.3044942
38. VDI Verein Deutscher Ingenieure e.V. (2021) VDI 2206 Entwicklungsmethodik für mechatronische Systeme. Beuth, Berlin
39. Dumstorff G, Paul S, Lang W (2014) Integration without disruption: the basic challenge of sensor integration. IEEE Sensors J 14(7):2102–2111. https://doi.org/10.1109/JSEN.2013.2294626
40. Bonaiti L, Knoll E, Otto M, Gorla C, Stahl K (2022) The effect of sensor integration on the load carrying capacity of gears. Machines 10(10):888. https://doi.org/10.3390/machines10100888
41. Peters J, Mirbach N, Herbst F, Riehl D, Kupnik M, Hofmann K, Matthiesen S (2024) Overcoming conflicts of objectives between sensory and mechanical domain in the development of sensor-integrating machine elements using the example of bolts. IEEE Access. https://doi.org/10.1109/ACCESS.2024.3423674
42. Peters J, Herbst F, Riehl D, Chadda R, Hofmann K, Kupnik M, Matthiesen S (2024) Sensorintegrierende schrauben: Bauraumidentifikation und -ausnutzung. In: Dresdner Maschinenelemente Kolloquium
43. Sahib MA, Ahmed BS (2016) A new multiobjective performance criterion used in PID tuning optimization algorithms. J Adv Res 7(1):125–134. https://doi.org/10.1016/j.jare.2015.03.004
44. Peters J, Menning JDM, Ewert A, Prokopchuk A, Breimann R, Herbst F, Riehl D, Doellken M, Henke E-FM, Wallmersperger T, Schlecht B, Kirchner E, Kupnik M, Hofmann K, Matthiesen S (2024) Design space optimization for sensor-integration in stan-

dardized machine elements. In: Proceedings of the ASME 2024 International Mechanical Engineering Congress and Exposition IMECE2024 https://doi.org/10.1115/IMECE2024-141505
45. Herbst F, Chadda R, Hartmann C, Peters J, Riehl D, Gwosch T, Hofmann K, Matthiesen S, Kupnik M (2022) Multi-axis force sensor for sensor-integrating bolts. In: 2022 IEEE Sensors. IEEE, Dallas, pp 1–4 https://doi.org/10.1109/SENSORS52175.2022.9967220
46. Herbst F, Chadda R, Peters J, Riehl D, Hartmann C, Suppelt S, Breimann R, Kirchner E, Hofmann K, Matthiesen S, Kupnik M (2024) Sensor-integrating bolt for multiaxial force measurement. IEEE Sensors J 24(17):27265–27274. https://doi.org/10.1109/JSEN.2024.3427833
47. Riehl D, Herbst F, Peters J, Leiacker D, Matthiesen S, Kupnik M, Hofmann K (2025) Flexible ultra-low power strain gauge readout platform for sensor-integrating bolts. In: 2025 IEEE International Instrumentation and Measurement Technology Conference (I2MTC), pp 1–6 https://doi.org/10.1109/I2MTC62753.2025.11078981
48. (2020) NXP: AN12365: NTAG 5—How to use energy harvesting. https://www.nxp.com/docs/en/application-note/AN12365.pdf. Accessed 10 Nov 2023
49. (2024) NGK Insulators: enerCera—Datasheet. https://www.ngk-insulators.com/en/product/enercera.html. Accessed 4 Feb 2025
50. Leiacker D, Riehl D, Korner D, Hofmann K (2024) Ultrasonic wake-up receiver for an ultra-low power communication platform. In: EASS 2024: Energieautonome Sensorsysteme. GMM-Fachbericht, vol 109, pp 34–36 (https://ieeexplore.ieee.org/document/10659673)
51. Korner D, Hofmann K (2022) An asic-based ultrasonic beacon sensor platform with energy selfsustaining communication for medical implants. In: EASS 2022: Energieautonome Sensorsysteme. GMM-Fachbericht, vol 102. VDE, Berlin Offenbach, pp 56–58 (https://ieeexplore.ieee.org/document/9899267)
52. Riehl D, Korner D, Keil F, Peters J, Matthiesen S, Hofmann K (2024) Flexible modular electronic platform for sensor-integrating bolts. In: EBL 2024: Elektronische Baugruppen und Leiterplatten. GMM-Fachbericht, vol 107. VDE, Berlin, pp 313–316
53. Bluetooth SIG Bluetooth Core Specification v5.4. https://www.bluetooth.com/specifications/specs/core54-html/. Accessed 29 Jan 2025
54. Bertocco M, Peruzzi G, Pozzebon A (2024) Performance measurements of lorawan connectivity for links through metallic shields: preliminary and feasibility tests. In: 2024 IEEE International Instrumentation and Measurement Technology Conference (I2MTC). IEEE, Glasgow, pp 1–6 https://doi.org/10.1109/I2MTC60896.2024.10560784
55. Gineprini M, Parrino S, Peruzzi G, Pozzebon A (2020) Lorawan performances for underground to aboveground data transmission. In: 2020 IEEE International Instrumentation and Measurement Technology Conference (I2MTC). IEEE, Dubrovnik, pp 1–6 https://doi.org/10.1109/I2MTC43012.2020.9128454
56. Seye MR, Ngom B, Gueye B, Diallo M (2018) A study of lora coverage: range evaluation and channel attenuation model. In: 2018 1st International Conference on Smart Cities and Communities (SCCIC). IEEE, Ouagadougou, pp 1–4 https://doi.org/10.1109/SCCIC.2018.8584548
57. Ott HW (2009) Electromagnetic compatibility engineering. Wiley, Hoboken
58. Peters J, Doellken M, Grauberger P, Herbst F, Riehl D, Kupnik M, Hofmann K, Matthiesen S (2025) Design support and strategies for integrating sensing functions into machine elements. Proc CIRP 136:522–527. https://doi.org/10.1016/j.procir.2025.08.090 (35th CIRP Design 2025)